Loss of Copine D Leads to Ras Activation in *Dictyostelium discoideum*

Cody T. Morrison[1,2], Sela K. Damer-Daigle[2], Bridget K. Plude[1,2], Allison G. Maillette[2], and Cynthia K. Damer[1,2,*]

1. Central Michigan University, Biochemistry, Cell & Molecular Biology Program
2. Central Michigan University, Department of Biology

* Correspondence: damer1ck@cmich.edu

Abstract

Copines are a family of calcium-dependent phospholipid-binding proteins found in most eukaryotes. The expression of multiple copine genes is dysregulated in various types of human cancers. Despite this, a common mechanistic function for copines remains unknown. We are studying copines in *Dictyostelium discoideum*, which has six copine genes (*cpnA*-*cpnF*). Cells lacking *cpnA* or *cpnC* (*cpnA*- and *cpnC*-, respectively) exhibit many phenotypes, including defects in development, chemotaxis, adhesion, and contractile vacuole (CV) function. To further characterize the function of copines, this study tested the hypothesis that CpnD is responsible for cellular functions distinct from CpnA and CpnC. In this study, we obtained two *cpnD* mutants that were generated via restriction enzyme-mediated integration (REMI) mutagenesis; one in the first exon (*cpnD(i291)*), and one in the second exon (*cpnD(i459)*) of the endogenous *cpnD* gene. Throughout our experiments, we found that *cpnD* mutants had increased cellular proliferation in both axenic and bacterial cultures. Additionally, we found that *cpnD* mutants exhibited precocious development and had significantly larger fruiting bodies than the parental cell line. We further investigated the morphology of *cpnD* mutants and found that they were significantly larger than parental cells and exhibited decreased cell-substrate adhesion. *cpnD* mutants also had increased activated Ras compared to the parental cell line, along with significantly smaller CVs, a phenotype that was rescued after PI3K inhibition. Finally, we found that GFP-tagged CpnD localizes to the leading edge of both randomly migrating cells and in cells responding to folate. This study is the first to describe copine proteins as having a regulatory function in Ras activation and downstream signaling effects. Additionally, this study further supports our hypothesis that copines act as nonredundant cellular proteins in *Dictyostelium* to regulate numerous processes.

Introduction

Copines are a family of evolutionarily conserved, calcium-dependent membrane-binding proteins found in a variety of eukaryotes ranging from unicellular organisms to humans (1). Copines are characterized by a conserved domain structure consisting of two N-terminal C2 domains and a C-terminal A domain that is similar to the von Willebrand factor A (VWA) domain found in integrins (1). The C2 domains function to facilitate calcium-dependent lipid binding (1,2), whereas the A domain serves as a protein-binding motif (2). Together, these domains suggest that copines act as calcium-responsive sensors that recruit or regulate proteins at membrane surfaces in response to intracellular calcium signals (2). Humans have nine copines encoded in their genome that exhibit differential expression throughout various tissue types. Dysregulated copine expression has been reported in numerous cancers and human diseases (3–8). Additionally, functional studies suggest that human copines play a role in promoting cell

proliferation, migration, and metastasis (9–11). Despite these associations, the molecular and cellular mechanisms by which copines regulate signaling pathways remain incompletely understood, highlighting the need for further investigations of copine function in vivo.

To address this, our lab aims to define the mechanistic function of copine proteins using the model organism *Dictyostelium discoideum*. *Dictyostelium* has six copine genes, while other model organisms either have no copine genes, like yeast and *Drosophila*, or only a few copine genes, like *C. elegans* (12). In their vegetative state, *Dictyostelium* exists as single-celled amoebae that feed on bacteria through phagocytosis; however, upon nutrient depletion, changes in gene expression initiate *Dictyostelium* to undergo development. Development begins when starving amoebae release cyclic AMP (cAMP) pulses, which act as a chemoattractant to initiate aggregation. Cells aggregate into mounds, which transform into migrating slugs. The slugs culminate into fruiting bodies that consist of a stalk supporting a spore head (13). Early development aggregation involves changes in cell migration and adhesion, both of which are processes reminiscent of cancer cells. Therefore, by leveraging *Dictyostelium's* unique biology, we aim to uncover the conserved copine functions relevant to both normal cellular processes and cancer progression.

Dictyostelium aggregation is a well-studied model of chemotaxis, where individual starving amoebae detect, relay, and move toward periodic pulses of cAMP. Chemotaxis is driven by a complex signal transduction network that converts the external cAMP signal into localized actin polymerization at the leading edge of the cell. Extracellular cAMP binds to G-protein coupled receptors (cAR1), which activate heterotrimeric G-proteins $G\alpha 2\beta\gamma$. This leads to the rapid activation of Ras proteins at the leading edge of migrating cells (14). Ras signals to downstream effectors like phosphoinositide 3-kinase (PI3K) to drive signaling cascades that are involved in the regulation of cell polarity, chemotaxis, F-actin dynamics, phagocytosis, and gene expression (15–19). Studies have shown that constitutively active RasC or RasG leads to hyperactivation of signaling pathways, resulting in increased cell spreading, cytoskeletal activity, and altered migration (20–24). Importantly, the mechanisms of Ras-mediated chemotaxis are conserved between *Dictyostelium* and mammalian cells. In mammalian cells, Ras signaling pathways also regulate cellular proliferation, growth, survival, and metabolism, and are frequently activated by mutations in cancer (23–26). As such, the Ras signaling pathway is often targeted for therapeutic interventions in cancer models (27).

The six copine genes (*cpnA-cpnF*) that encode proteins CpnA-CpnF in *Dictyostelium* exhibit 28-60% amino acid identity and distinct expression patterns throughout development, suggesting that they perform nonredundant functions (12,28). In a previous study, we characterized the calcium-dependent lipid binding properties and localization of all of the copine proteins except CpnD (29). Each copine had distinct calcium-dependent phospholipid binding properties, along with variable timing and magnitude of membrane localization from the cytosol upon cAMP stimulation. Additionally, GFP-tagged CpnB, CpnC, and CpnF exhibited both cytoplasmic and

nuclear localization, while CpnA and CpnE were cytosolic (29). Studies with *cpnA* null (*cpnA*-) cells have revealed numerous cellular phenotypes, including defects in chemotaxis, adhesion, cytokinesis, contractile vacuole (CV) function, development, and phosphatidylserine (PS) exposure (28,30–33). *cpnA*- cells also showed increased cytosolic calcium concentrations, indicating a role for CpnA in calcium homeostasis (33). *cpnC*- cells exhibited different cellular phenotypes, including defects in chemotaxis, adhesion, and development (34). *cpnC*- cells also exhibited significantly reduced RegA, a cAMP phosphodiesterase important in cAMP signaling (34). In this study, we describe the phenotypic analysis of *cpnD* mutants. Here, we show that *cpnD* mutants display distinct defects in morphology, growth, development, and CV size, along with increased Ras activation. Furthermore, we have now been able to characterize the cellular localization of CpnD. Therefore, each copine appears to differentially influence key signaling mechanisms, suggesting that copines act as modulators of intracellular communication.

Results

cpnD mutants have increased proliferation in both axenic and bacterial cultures

To study the function of CpnD in *Dictyostelium*, we obtained two *cpnD* mutant cell lines and the parental (AX4) strain from the *Dictyostelium* Stock Center (35). The *cpnD* mutants were created as part of a REMI-seq project to generate a genome-wide mutant resource for *Dictyostelium* (36). The *cpnD* mutants contain a 1,589 bp insert in the first (*cpnD(i291)*) or second (*cpnD(i459)*) exon of the endogenous *cpnD* gene, respectively (Figure 1A). We isolated clonal populations of each cell strain and confirmed the presence and location of the REMI insertions in each mutant via PCR and whole-genome sequencing.

To determine if the mutants exhibited normal proliferation, we performed growth assays with both the parental and *cpnD* mutant cell lines. Cells were grown in a shaking suspension, and cell samples were collected and counted using a hemocytometer each day for 7 days. Both *cpnD(i291)* and *cpnD(i459)* cells appeared to proliferate faster than the parental cell line, but only the *cpnD(i291)* cells were significantly different from the parental AX4 cells (Figure 1B). We also examined cell proliferation on bacterial lawns. AX4 cells and *cpnD* mutants were plated on SM/5 agar with *E. coli B/R*. As the *Dictyostelium* feed on the *E. coli B/R*, clear plaques arise within the bacterial lawn. Images were taken of the plaques on days 3, 4, and 5 after plating. The plaques created by the *cpnD* mutants appeared before AX4 plaques and were noticeably larger than the parental AX4 plaque on day 3 (Figure 1C). As cells consume the bacteria at the edge of the plaque, cells within the plaque starve and go through development to form fruiting bodies. On day 4, both *cpnD* mutants had begun development with the formation of mounds and slugs, while AX4 cells had not yet formed multicellular structures. On day 5, AX4 cells had formed mounds and a few fruiting bodies, while the *cpnD* mutants had formed mostly fruiting bodies (Figure 1C). These data indicate that *cpnD* mutants proliferate faster in both axenic culture and bacterial cultures.

cpnD mutants exhibit precocious development and have larger fruiting bodies than parental cells

We next investigated whether *cpnD* mutants exhibited normal developmental morphology and timing by monitoring the synchronized development of both the *cpnD* mutants and parental AX4 cells. Parental and *cpnD* mutants in starvation buffer were plated on nitrocellulose filters, and images were captured throughout a 48-hour timeframe. Representative images of all three cell lines are shown at 4 different timepoints in Figure 2A. At 6 hr, none of the three cell lines displayed multicellular structures. At 18 hr, AX4 cells had formed small mounds. In contrast, *cpnD(i459)* cells had progressed beyond the mound stage and formed large slugs, while the *cpnD(i291)* cells were at an intermediate stage of development, forming large mounds with some beginning to tip and transition into slugs. These observations indicate that both *cpnD* mutants develop more rapidly than AX4 cells, with *cpnD(i459)* cells developing faster than *cpnD(i291)* cells. Additionally, both *cpnD* mutants appeared to form larger mounds, slugs, and fruiting bodies compared to AX4 cells (Figure 2A). To quantify these differences, we measured the area of fruiting body spore heads ($n > 700$ across two trials) using ImageJ. Both *cpnD* mutants produced significantly larger spore heads than AX4, with *cpnD(i459)* forming significantly larger spore heads than *cpnD(i291)* (Figure 2B).

cpnD mutant cells are significantly larger and flatter than the parental cell line

Upon morphological inspection of the *cpnD* mutant cells, we noticed that some of the mutant cells appeared flatter and “pancake”-shaped compared to the parental AX4 cell line. To quantify these observations, we imaged cells using differential interference contrast (DIC) microscopy and measured the cell area. On average, both the *cpnD* mutants had a significantly larger mean cell area than the parental cell line. Interestingly, *cpnD(i459)* cells were the largest cell type and significantly differed in size from the *cpnD(i291)* cells (Figure 3A, 3B).

cpnD mutants have decreased cell-substrate adhesion

The flatter, “pancake”-like morphology of the *cpnD* mutant cells suggested that *cpnD* mutants may have altered substratum adhesion; increased and decreased adhesion have both been shown to lead to a flatter morphology (37,38). To test this, parental and *cpnD* mutants were allowed to adhere to Petri dishes, then rotated at 3 speeds (50, 75, and 100 RPM). After each rotation, the media was replaced to remove detached cells. Three marked locations on the dish were imaged using phase contrast microscopy to assess the number of cells that remained adhered to the dish. We found that both *cpnD* mutants showed significantly reduced adhesion to the Petri dish at 50 and 75 RPM compared to the parental cell line (Figure 4A). There were no significant differences in cell-substrate adhesion between the parental and *cpnD* mutant cell lines at 100 RPM, suggesting that the forces inflicted on the cells at high RPM are greater than the adhesion strength of *Dictyostelium*.

SibA is a transmembrane protein essential for cell-substrate adhesion in *Dictyostelium* and has been shown to affect cellular adhesion based on its expression (39). We have previously shown that *cpnC*- cells have significantly decreased cell-substrate adhesion and reduced SibA expression (34). To determine if the decreased cell-substrate adhesion in *cpnD* mutants may be due to changes in SibA expression, whole-cell samples of parental and *cpnD* mutant cells were analyzed by Western blot to determine levels of SibA expression. SibA expression was reduced in both *cpnD* mutants compared to parental cells (Figure 4B). Because the α-SibA antibody recognizes an additional protein, we have previously performed Western blotting with *sibA* null cells to verify that the higher molecular weight band is SibA (34).

cpnD mutant cells have increased levels of activated Ras

The flatter, pancake-like cellular morphology has been observed in cells that have increased activation of RasC (23), possibly due to the activation of the actin cytoskeleton, causing cells to create protrusions and spread out (40). Additionally, research has shown that global activation of Ras by recruitment of GefA to the cellular membrane promotes cell spreading (41). Because our *cpnD* mutants were significantly larger and flatter than the parental cell line, we wanted to test whether the *cpnD* mutants had increased activated Ras. To test this, we performed an activated Ras pulldown assay. Normally, vegetative cells that have not been starved and have not been stimulated with cAMP show very little Ras activation (15). However, our vegetative *cpnD* mutants did have significantly higher levels of active Ras compared to the parental strain, while the levels of total Ras between all cell lines were not significantly different (Figure 5).

PI3K inhibition suppresses the small CV defects observed in *cpnD* mutants

We had also noticed that *cpnD* mutants exhibited smaller contractile vacuoles than AX4 cells. Contractile vacuoles are intracellular organelles involved in the regulation of water and various ions in numerous cells, including *Dictyostelium* (42). After searching the literature for examples of Ras overactivation associated with CV phenotypes, we found that researchers looking for mutants with high levels of constitutively active PI3K identified the gene for *sodC* that encodes a superoxide dismutase. *sodC*- cells exhibited more active Ras than parental cells, similar to *cpnD* mutants (43). In addition, *sodC*- cells made smaller than normal CVs that could be rescued with PI3K inhibitor, LY294002 (43). To determine whether LY294002 could suppress the small CV defect observed in the cpnD mutants, we performed CV assays with our LY294002-treated and untreated parental AX4 and *cpnD* mutant cell lines. Cells were allowed to adhere to glass-bottom dishes and then incubated in water with or without LY294002 before performing DIC microscopy to measure CV area. The mean CV area of the *cpnD* mutants was smaller compared to AX4 (Figure 6A, 6B). When we treated the cells with LY294002, the mean CV area of the *cpnD* mutant cell lines significantly increased, while the CV area of the parental AX4 strain did not change (Figure 6A, 6B). These experiments indicate that the flat morphology and small CV defects observed in *cpnD* mutants are due to increased activation of the Ras/PI3K

signaling pathway.

GFP-tagged CpnD localizes to the leading edge of *Dictyostelium* in both randomly migrating cells and in response to folate

We have previously shown that GFP-tagged copines (besides CpnD) exhibit both cytosolic and nuclear localization in live cells (29). In fixed cells, and in response to cAMP stimulation, GFP-tagged copines transiently translocated from the cytosol to the plasma membrane and to various intracellular organelle membranes (29). Because our *cpnD* mutant cells were significantly larger and flatter than the parental AX4 strain, we hypothesized that CpnD may play a role in cellular polarity and migration. To test this, we subcloned the cDNA for *cpnD* into the pTX-GFP vector at the *SacI* site for the overexpression of CpnD tagged with GFP at the N-terminus (GFP-CpnD). The plasmids were transformed into parental *Dictyostelium* cells, and the expression of GFP-tagged CpnD was verified by Western blot.

Parental cells expressing GFP-tagged CpnD were plated on glass-bottom dishes in VL-6 media. Immediately before time-lapse confocal microscopy, the VL-6 media was replaced with starvation buffer before live-cell imaging. Throughout the two-minute time-lapse, GFP-CpnD localized to the leading edge of the cells as they were allowed to migrate freely (Figure 7A). Parental cells expressing GFP-tagged CpnD were also used in an under-agar folate chemotaxis assay, which was visualized using time-lapse confocal microscopy. During this time-lapse, GFP-tagged CpnD localized to the leading edge of the parental cell in the direction of the folate (Figure 7B, arrow). During this time, the localization of GFP-tagged CpnD was only in the direction of folate, and did not move to any other area of the cell during time-lapse imaging like was seen in randomly migrating cells (Figure 7A).

Discussion

We have previously shown that CpnA and CpnC are involved in numerous cellular functions in *Dictyostelium*. To further characterize the function of copines, this study tested the hypothesis that CpnD is responsible for cellular functions distinct from CpnA and CpnC. The two *cpnD* mutants we received from the *Dictyostelium* Stock Center differed in the location of their insertional mutagenesis (Figure 1A). The *cpnD(i291)* cell line contains the REMI insert within the first exon of the endogenous *cpnD* gene, while the *cpnD(i459)* cell line contains the REMI insert in the second exon. Therefore, the *cpnD(i459)* cell line may potentially express a partial protein containing the complete first C2 domain. Therefore, we initially hypothesized that the phenotypic defects of the *cpnD(i291)* mutant may be more drastic compared to the *cpnD(i459)* mutant because the proteins may be partially functional. However, we found the opposite; the phenotypic defects seen in the *cpnD(i459)* mutant were more severe than those of the *cpnD(i291)* mutant. The more severe phenotype of the *cpnD(i459)* mutant is most likely due to a dominant negative effect where the truncated protein containing only the first C2 may be able to bind target proteins, but lacks function, thereby preventing other proteins from also binding to the same targets.

Throughout our characterization, we observed numerous phenotypes in our *cpnD* mutants compared to the AX4 parental cell line. We hypothesize that these phenotypes could all be attributed to increased activated Ras, which has been shown to mediate the recruitment and activation of PI3K (44) and subsequently increase PIP3 levels. Our results showed that *cpnD* mutants phagocytosed bacteria more quickly than the parental AX4 cells. Studies in macrophages and *Dictyostelium* have shown that PI3K inactivation interferes with phagocytosis of bacteria, large particles, and micropinocytosis (45,46). Additionally, studies have shown that PI3K is an important component of leukocyte phagocytosis and the regulation of superoxide species (47). Similar studies investigating the role of activated Ras and PI3K on superoxide dismutase have been done in *Dictyostelium* cells lacking superoxide dismutase (*sodC*-), which has been shown to regulate Ras (43). Cells lacking *sodC* showed higher levels of activated Ras, smaller CVs, and significantly larger CVs upon LY294002 treatment (43). Our CV defect results suggest that the *cpnD* mutants have increased PI3K levels as a result of increased activated Ras. Upon treatment with LY294002, both *cpnD* mutant cell lines had significantly larger CV area compared to no treatment. Furthermore, it has been shown that cells lacking C2GAP2 showed an increase in Ras activation, leading to elevated phagocytosis and cell growth (48). These results collectively support our hypothesis that *cpnD* mutants have higher levels of PI3K as a result of more activated Ras, which could explain why the *cpnD* mutants were growing and developing faster in axenic and bacterial cultures.

This study showed that *cpnD* mutants exhibited precocious growth and development compared to the parental AX4 cell line. The increased cellular size or “pancake”-like morphology is also likely due to higher levels of activated Ras and PI3K (23). Because Ras and PI3K pathways have been shown to regulate vegetative growth, cytokinesis, and morphology of *Dictyostelium* (49,50), the enlarged morphological phenotype seen in *cpnD* mutants may reflect elevated levels of active Ras and PI3K. If the levels of active Ras and PI3K are higher in vegetative *cpnD* mutants, this increased activity could impact developmental gene expression changes and explain why the developmental processes of *cpnD* mutants are also precocious compared to the parental cell line. Our results also showed that *cpnD* mutants were less adhesive than the AX4 parental strain. Previous studies have discussed the importance of Rap1 in coordinating chemotaxis and adhesion in *Dictyostelium* (51,52). Studies have also shown that PI3K directly interacts with Rap1 to regulate phosphatidylinositol (3,4,5)-triphosphate (PIP3) formation and subsequent cellular adhesion, and RasG activation is essential for regulating PIP3 signaling (40,53). Furthermore, Rap1 activation in response to cAMP has been shown to occur downstream of RasG (40). Because we hypothesize that CpnD is a negative regulator of the Ras-PI3K pathway in *Dictyostelium*, Ras hyperactivation could overactivate PI3K and disrupt normal Rap1 adhesion dynamics. If activated Ras was disrupting this pathway, it would explain why our *cpnD* mutant cells exhibit adhesion defects compared to the AX4 parental strain.

We have previously characterized the cellular localization of copines using GFP-tagged copines in parental *Dictyostelium* cell lines (29). However, at the time of our previous study, we were not able to obtain GFP-tagged CpnD. In this study, we have

successfully created a GFP-tagged CpnD to characterize its cellular localization. In both random migration and migration in response to folate, we observed GFP-CpnD localizing to the leading edge of parental cells. Because of these results, we hypothesize that CpnD localizes to the leading edge of migrating cells to regulate Ras and PIP3 activity. It has been shown that Ras signaling localizes to the leading edge of *Dictyostelium* to regulate cell polarity and cell movement (50,54). We hypothesize that CpnD may act as a positive regulator of a GTPase-activating protein (GAP) or negatively regulate a guanine exchange factor (GEF). If CpnD functions to bind to a GAP to turn Ras activation down, it would explain why the levels of activated Ras are higher in the *cpnD* mutants and lower in the AX4 parental strain. Conversely, CpnD may function as a negative regulator of Ras by binding to GEF in parental AX4 cells to keep overactive Ras levels low. This hypothesis is supported by previous work showing that mammalian Copine-6 is capable of binding, activating, and recruiting Rho GTPase Rac1, a member of the Ras superfamily, to cellular membranes (55).

Together, this study is the first to describe copine proteins as having a regulatory function in Ras activation and its subsequent downstream signaling effects. Additionally, this study further supports our hypothesis that copines act as nonredundant cellular proteins in *Dictyostelium* to regulate numerous processes. In genetic cancer screenings, it has been shown that numerous copine genes are dysregulated (3). Additionally, studies have shown that constitutively active Ras leads to downstream signaling pathway dysregulation, and mutations that cause constitutively active Ras are highly prevalent in human cancers (24,26). Therefore, understanding the biological role of copines could add to our understanding of how cancer progresses, as well as pursue new therapeutic interventions.

Methods

Dictyostelium cell culture

The parental axenic strain (AX4) and the *cpnD* mutants were obtained from the *Dictyostelium* Stock Center (35). AX4 and *cpnD* mutants were grown on plastic Petri dishes at 18 °C in VL-6 media (Formedium, VL60102) supplemented with penicillin-streptomycin (60 U/mL). *cpnD* mutants were cultured in media containing blasticidin (30 µg/mL, InvivoGen, ant-bl-1). The *cpnD* mutant cell lines were generated via restriction enzyme-mediated integration (REMI) and are part of the genome-wide *Dictyostelium* insertion (GWDI) bank (36). *cpnD* mutant cell lines consist of a 1,589 bp REMI insert containing a blasticidin-resistant gene (*bsr*) inserted into the first (291 bp) or second (459 bp) exon of the endogenous *cpnD* gene to create the *cpnD(i291)* and *cpnD(i459)* cells, respectively. The cDNA for *cpnD* was subcloned into the *SacI* site of the pTX-GFP plasmid (29,56). The plasmid was electroporated into NC4A2 and AX4 parental cell strains. Cells were pulsed twice with a 5 second interval at 0.85 kV. Cells were placed on ice for 5 minutes and then plated in VL-6 media. Transformants were selected using G418 (geneticin) at 60 µg/mL after 24 hours. Expression of GFP-CpnD was verified with a Western blot using an α-GFP antibody ((29); Santa Cruz sc-9996).

Growth assay

AX4 and *cpnD* mutant cell lines were harvested from plates and placed in 125 mL flasks containing 12.5 mL of VL-6 media with 60 U/mL penicillin-streptomycin. Flasks containing a starting concentration of 5 x 10^4 cells/mL were placed in a shaking incubator set to 125 RPM at 18 °C. Every 24 hours for 7 days, three samples per cell line were removed from each flask, and cell densities were estimated using a hemocytometer. The cell densities of the three samples from each flask were averaged. Three growth assay trials were performed, and the mean cell densities on each day were averaged. To determine significant differences between cell growth in AX4 and *cpnD* mutant cells, a repeated measures ANOVA with Tukey's post hoc multiple comparisons test was performed.

Developmental assays

AX4 and *cpnD* mutant cell lines were harvested from plates, counted using a hemocytometer, and centrifuged at 437 x g for 5 minutes at 4 °C. Cell pellets were washed twice with ice-cold developmental buffer ((DB), 5 mM Na_2HPO_4, 5 mM KH_2PO_4, 1 mM $CaCl_2$, 2 mM $MgCl_2$, pH 6.5), and resupended to obtain 5 x 10^7 cells/mL. Cells (2.5 x 10^7) were plated on black filters (catalog no. HABP04700; Millipore), placed on DB-soaked pads in dishes (catalog no. 09-753-53C; Fisher), and allowed to develop for 48 hours. Images were taken using a Nikon SMZ800N dissecting microscope every two hours for 28 hours, followed by a 48-hour image to observe mature fruiting bodies. Two developmental assays were performed, and representative images for each cell line were chosen. The area of the spore heads from each cell line (n > 700) across two trials was measured using ImageJ. Individual fruiting body measurements were graphed for each cell line after removing outliers. A one-way ANOVA with Tukey's post hoc multiple comparisons test was performed to determine statistical significance between the AX4 and *cpnD* mutant cell lines.

For developmental assays on bacterial lawns, *E. coli B/R* was inoculated into 2 mL of VL-6 without penicillin-streptomycin and incubated at 220 RPM at 37 °C for 16 hours. AX4 and *cpnD* mutant cell lines were harvested from Petri dishes and counted using a hemocytometer and subjected to serial dilutions to obtain a final concentration of 500 cells/mL. *E. coli B/R* (500 µL) and *Dictyostelium* cells (100 µL) were spread on SM/5 agar plates (0.2% proteose peptone 2, 0.2% yeast extract, 0.2% glucose, 0.2% $MgSO_4 \cdot 7\ H_2O$, 0.19% KH_2PO_4, 1% K_2HPO_4, 1.5% agar, pH 6.4). Plates were incubated at 18 °C and examined for plaque formation. Plates were imaged with a Nikon SMZ800N dissecting microscope on days 3, 4, and 5.

Cell size and fruiting body measurements

AX4 and *cpnD* mutant cells were harvested from plates, counted using a hemocytometer, and centrifuged at 437 x g for 5 minutes at 4 °C. The cell pellet was resuspended in VL-6 media at 2 x 10^6 cells/mL. On glass-bottom dishes, 200 µL of the cell suspension was plated and allowed to adhere for 20 minutes. Cells were then

imaged using a TE2000-S Nikon Eclipse microscope with a 60X oil objective and differential interference contrast (DIC) microscopy. The area of individual cells from each cell type (n > 700) across two trials was measured using ImageJ, and individual cell measurements were graphed for each cell type after removing outliers. A one-way ANOVA with Tukey's post hoc multiple comparisons test was performed to determine statistical significance between the AX4 and *cpnD* mutant cell lines.

Adhesion assay

AX4 and *cpnD* mutant cells were harvested from plates, counted using a hemocytometer, and centrifuged at 437 x g for 5 minutes at 4 °C. The cell pellets were resuspended in VL-6 media at 1 x 10^6 cells/mL. On 60 mm Petri dishes, 2 mL of each cell type was allowed to adhere for 30 minutes. The cells that had not adhered to the plates were removed, and the media was replaced with fresh media. Images of the adhered cells were taken on a Nikon TE2000 microscope with a 20X phase-contrast objective at three marked spots on the Petri dishes. Cells on plates were rotated for 15 minutes at 50 RPM. Detached cells were removed from the plates, and new media was added. New images at each marked spot were captured. This procedure was repeated at 75 and 100 RPM. The number of cells in each image was counted using the ImageJ Cell Counter plugin, and counts were averaged. The percentage of detached cells after each rotation was calculated by the difference of the average number of cells remaining after rotation from the average number of cells present before rotation, divided by the number of cells present before rotation. Data from five trials were averaged and analyzed for significant differences between AX4 and *cpnD* mutant cells by a two-way ANOVA with uncorrected Fisher's LSD post hoc test.

Ras activation assay

AX4 and *cpnD* mutant cells were harvested from plates, counted using a hemocytometer, and centrifuged at 437 x g for 5 minutes at 4 °C. The cell pellets were resuspended in VL-6 media at 4 x 10^6 cells/mL. To assess Ras activity in the AX4 and *cpnD* mutant cells, we used an activated Ras pull-down assay kit (#BK008-S, Cytoskeleton Inc) following the manufacturer's protocol, with the exception that 4 x 10^6 cells/mL were used for the pull-down assays. Data from three and four trials were averaged for the activated Ras and total Ras, respectively. The data were analyzed for significant differences by a one-way ANOVA with Tukey's post hoc multiple comparisons test.

Western blot

AX4 and *cpnD* mutant cells were harvested from plates, counted using a hemocytometer, and centrifuged at 437 x g for 5 minutes at 4 °C. The cell pellets were resuspended in sample buffer (0.2 M Tris-HCl, 0.4 M DTT, 277 mM SDS, 6 mM Bromophenol blue, 4.3 M Glycerol), and 2 x 10^6 cells were loaded into the stain-free gels (BIO-RAD, 4568034) and run for 2 hours at 100 volts. After electrophoresis, the stain-free gels were imaged using a BIO-RAD ChemiDoc Touch Imaging System. The

stain-free gels were then transferred to a polyvinylidene difluoride (PVDF) membrane (ThermoFisher Scientific, 88518) for 1 hour at 100 volts. The membranes were placed in Blotto (5% dried milk in 1% (v/v) Tween-20 in phosphate-buffered saline (PBS-T)) for 30 minutes, and then incubated with α-RegA (1:4000) polyclonal antibody (gift from Robert Kay; (57)), α-SibA (1:1000) polyclonal antibody (Geneva Antibody Facility) for 2 hours at room temperature, or α-Pan Ras (1:250) mouse monoclonal primary antibody (#BK008-S, Cytoskeleton) for 3 hours at room temperature. The membranes were washed three times for 5 minutes with PBS-T. After washing, the membranes were incubated with an α-rabbit HRP-conjugated secondary antibody (1:15,000) or an α-mouse HRP-conjugated secondary antibody (1:15,000) for 1 hour at room temperature in Blotto. The membranes were washed three times for 10 minutes with PBS-T. Membranes were imaged on the BIO-RAD ChemiDoc Touch Imaging system using Femtoglow HRP substrate (Michigan Diagnostics, FWPS02).

Western blot densitometry

For densitometry analysis of SibA, band densities were measured using Image Lab v6.1 from BIO-RAD. Each band density of the Western blot image was measured and then normalized to the density of all proteins in the corresponding lane from the stain-free gel image. Normalized Western blot band densities were further normalized to the average adjusted total band volume intensities across all lanes. Western blot and gel images from six trials were analyzed, and normalized band densities were averaged and analyzed for significant differences using a one-way ANOVA with Tukey's post hoc multiple comparisons test.

For densitometry analysis of total Ras alone, each band density of the Western blot image was measured and then normalized to the density of all proteins in the corresponding lane from the stain-free gel image. Normalized Western blot band densities were further normalized to the average adjusted total band volume intensities across all lanes. Western blot and gel images from four trials were analyzed, and normalized band densities were averaged and analyzed for significant differences using a one-way ANOVA with Tukey's post hoc multiple comparisons test.

For densitometry analysis of active Ras, band densities of active Ras and total Ras were measured using Image Lab v6.1 from BIO-RAD. The adjusted total band volume densities of the active Ras bands were normalized to the average adjusted total band volume intensities across all active Ras lanes, and the same was done for total Ras as described above. Normalized active Ras band densities were further normalized to the normalized adjusted total band volume intensities of their respective total Ras samples. Western blot images from three trials were analyzed, and normalized band densities were averaged and analyzed for significant differences using a one-way ANOVA with Tukey's post hoc multiple comparisons test.

Contractile vacuole assay

AX4 and *cpnD* mutant cells in VL-6 media (2 x 10^6 cells/mL) were plated on 35 mm

glass-bottom dishes and allowed to adhere for 20 minutes. The media was removed and replaced with water or water with 25 μM LY294002 (Cell Signaling Technologies, #9901S). After a two-hour incubation period, the cells were imaged using a TE2000-S Nikon Eclipse microscope with a 60X oil objective and differential interference contrast (DIC) microscopy. The area of each contractile vacuole (n > 209 CVs/cell type) was measured using ImageJ, outliers were removed, and a one-way ANOVA with Šídák's post hoc multiple comparisons test was performed to analyze significant differences between AX4 and each of the *cpnD* mutant cells, as well as differences between cell types and LY294002 treatment.

GFP-tagged CpnD assays

For random movement assays using time-lapse confocal microscopy, cells containing the GFP-CpnD plasmid were harvested from plates, counted using a hemocytometer, and centrifuged at 1500 437 x g for 5 minutes. The cells were resuspended in VL-6 media at 2 x10^6 cells/mL. In 35 mm glass-bottom dishes, 200 μL of cell suspension was plated and allowed to adhere for 20 minutes. The VL-6 media was then replaced with DB before imaging.

For under agar chemotaxis assays using time-lapse confocal microscopy, 35 mm glass-bottom dishes were incubated with bovine serum albumin ((BSA) 10% in water) for 8 minutes, rinsed, and allowed to dry. Agarose (1%) was added to SM media (1% glucose, 1% proteose peptone, 0.1% yeast extract, 0.05% $MgSO_4$, 0.19% KH_2PO_4, 0.06% K_2HPO_4, pH 6), melted, and then 2 mL was added to each plate. After solidification, a rectangular trough in the center of the plate was cut out of the agarose, and two holes were made 5 mm from the trough with a plastic straw. Cells expressing GFP-tagged CpnD were harvested from plates and centrifuged at 437 x g for 5 minutes. Cells were resuspended in SM media at 5 x 10^6 cells/mL, and 30 μL was added to each hole in the agarose plate. A 100 mM folic acid stock was prepared, and 100 μL of the stock was added to 900 μL of warmed SM agarose. The mixture was added to fill the rectangular trough. A coverslip was placed over the center of the plate to cover the holes. Migrating cells were imaged 2-5 hours later.

Acknowledgements

We thank Central Michigan University's flow cytometry and imaging facilities. This research was funded by NIH, grant number 2R15GM078089-03 (CKD). Additional funding was provided by Central Michigan University's Department of Biology and the College of Science and Engineering.

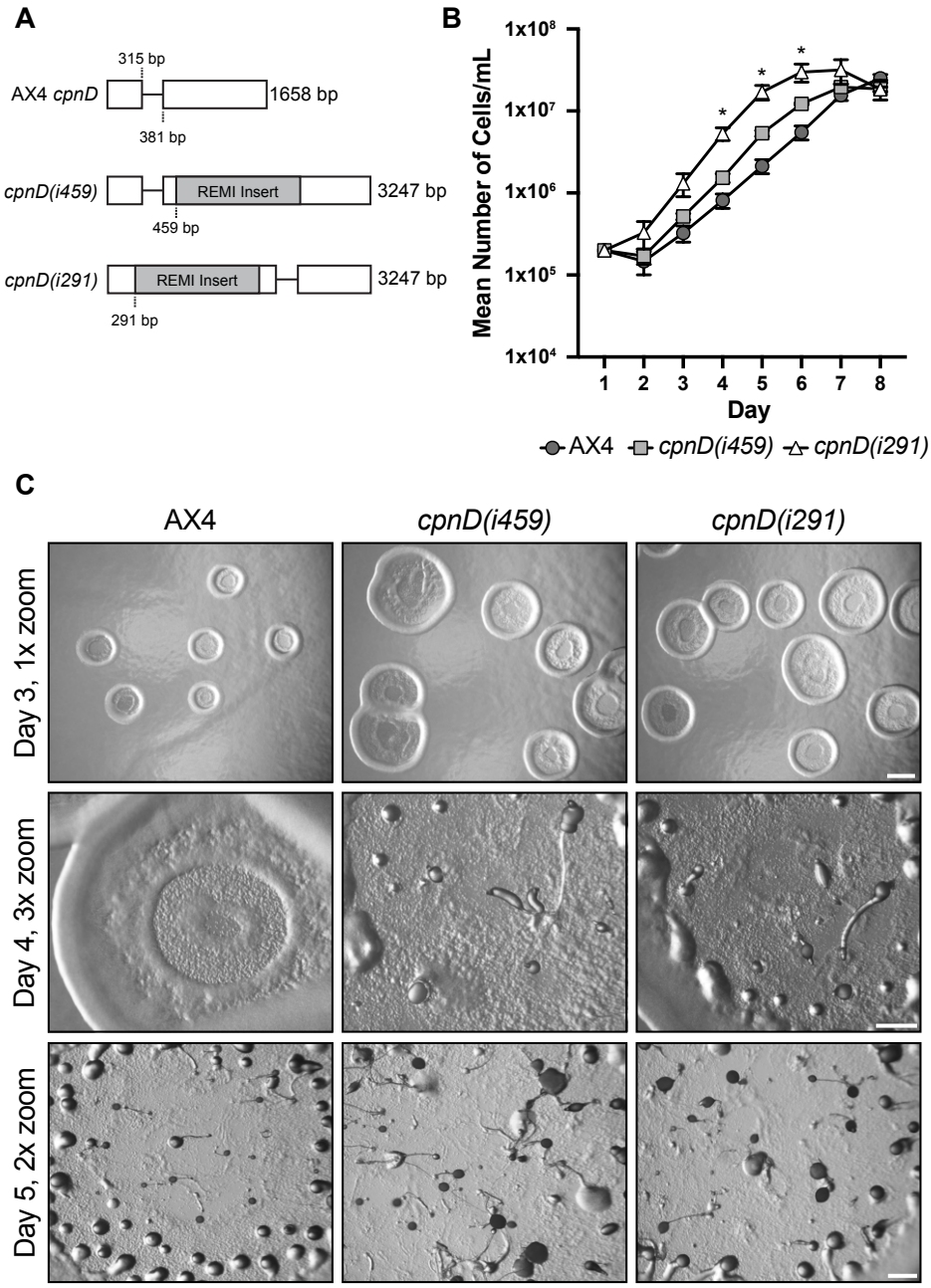

Figure 1. *cpnD* mutants have increased proliferation in both axenic and bacterial cultures. (A) Both *cpnD* mutant strains contain a 1,589 bp REMI insert in the first (*cpnD(i291))* or second (*cpnDi(459))* exon of the endogenous AX4 *cpnD* gene. (B) AX4 cells and both *cpnD* mutants were grown in a shaking suspension starting at a cellular density of 5 x 10^4 cells/mL. Cell densities were counted and averaged once a day for 7 days using a hemocytometer. Mean cell densities were calculated from three trials, and a repeated measures ANOVA with Tukey's post hoc multiple comparisons test was performed to analyze significant differences between cell lines. * indicates a significant difference between the parental AX4 cell line and *cpnD(i291)*, $p < 0.05$. (C) AX4 and *cpnD* mutant cells were plated with *E. coli B/R* on SM/5 agar. Plaques were imaged

after 3, 4, and 5 days after plating, and representative images are shown. Day 3 scale bar = 1000 μm. Day 4 and 5 scale bars = 500 μm.

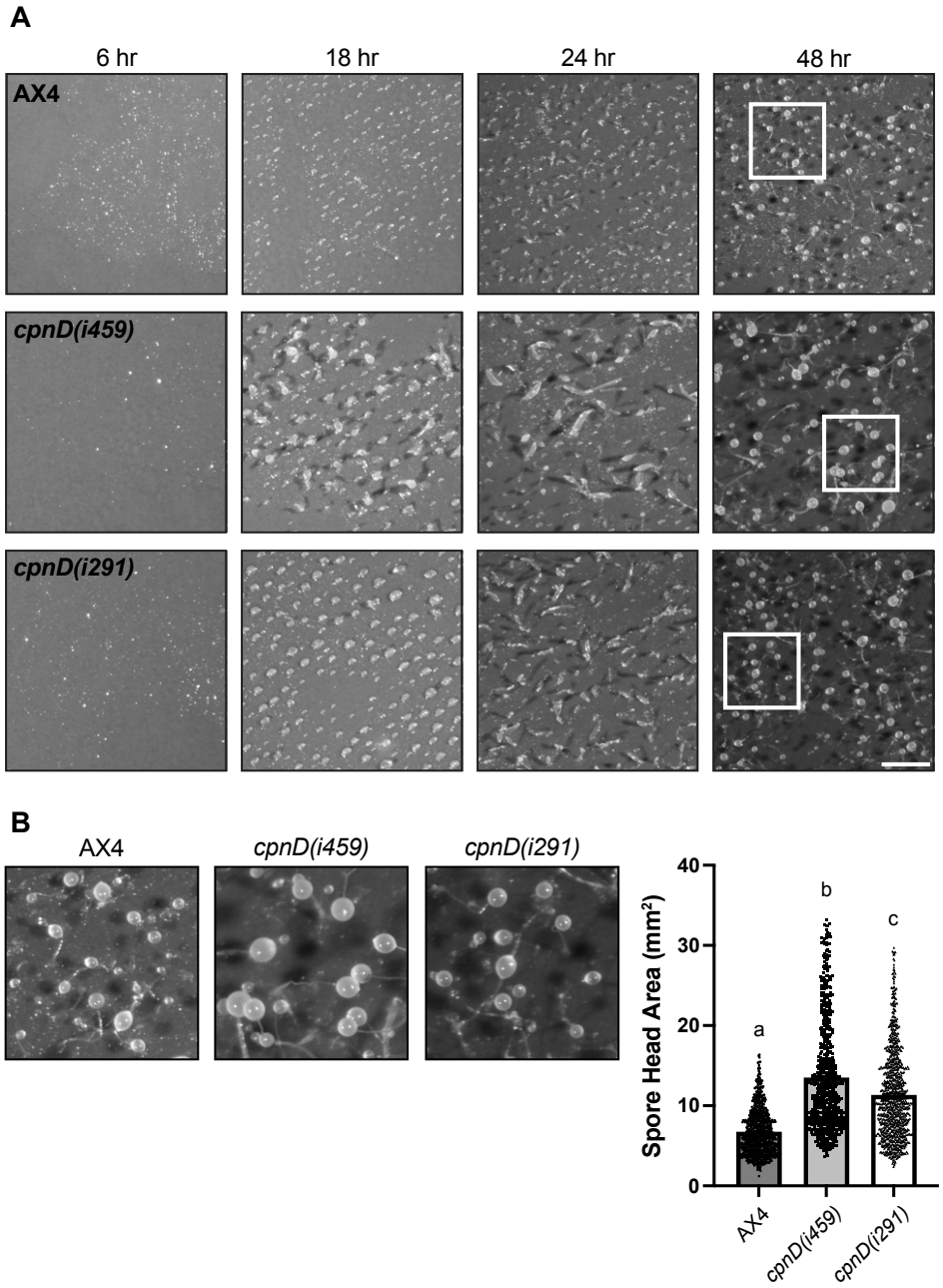

Figure 2. *cpnD* mutants exhibit precocious development and have significantly larger fruiting bodies. (A) AX4 and *cpnD* mutant cells were resuspended in starvation buffer and plated on nitrocellulose filters to synchronize developmental timing. Representative images across two trials are shown throughout a 48-hour imaging window. At 6 hr, none of the cell lines exhibited multicellular characteristics. At 18 hr, AX4 cells formed small mounds, while *cpnD(i459)* mutants formed large slugs and *cpnD(i291)* formed large mounds with some slugs. At 24 hr, AX4 cells formed slugs, while both *cpnD* mutants formed larger slugs and showed occurrences of fruiting body formation. At 48 hr, all three cell lines reached their terminal developmental timepoint, exhibiting fruiting bodies of various sizes. Scale bar = 1 mm. (B) Insets from white boxes

shown in Figure 2A of AX4 and *cpnD* mutant cells at 48 hr developmental time point. The bar graph represents the area of fruiting body spore heads (n > 700 across two trials) measured using ImageJ. Data were analyzed for significant differences using a one-way ANOVA with Tukey's post hoc multiple comparisons after removing outliers. Different letters above the bars indicate a significant difference, $p < 0.0001$.

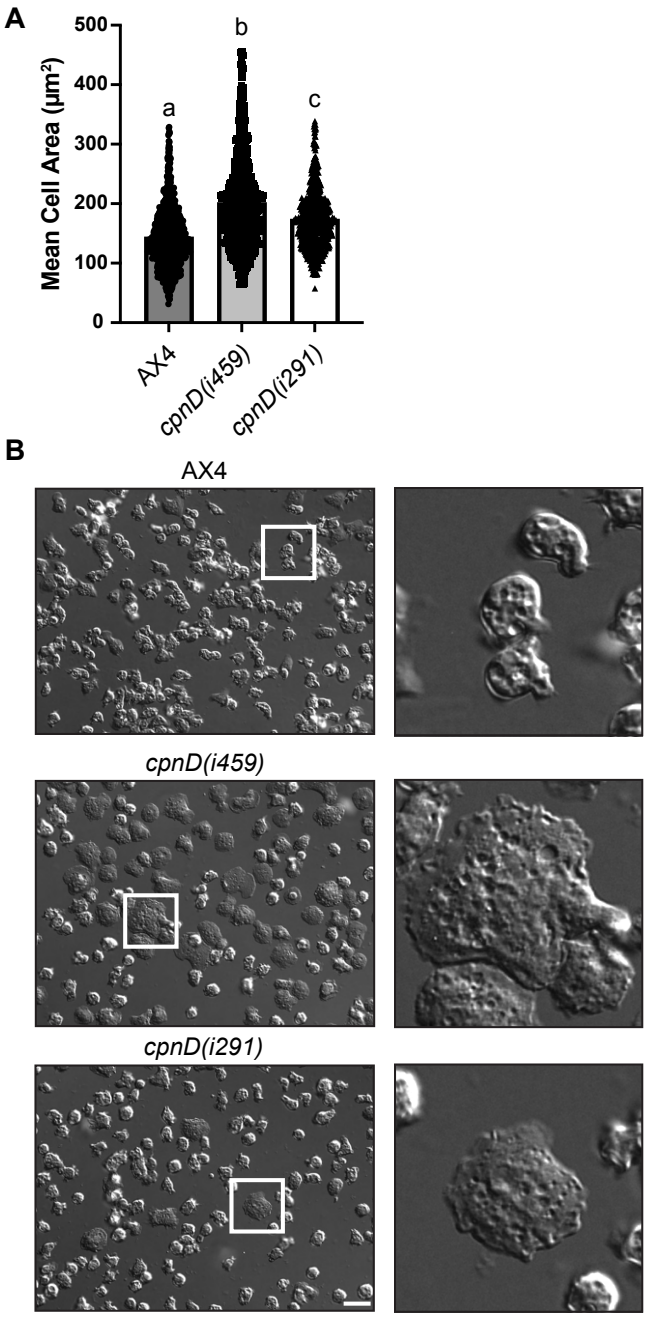

Figure 3. *cpnD* mutants have a larger cell area than parental cells. (A) The mean cell area of AX4 and *cpnD* mutants (n > 700 cells across two trials) was measured using ImageJ, and the bar graph represents individual cell measurements. Data were analyzed for significant differences using a one-way ANOVA with Tukey's post hoc multiple comparisons after removing outliers. Different letters above the bars indicate a significant difference, $p < 0.0001$. (B) AX4 and *cpnD* mutants were plated on glass-bottom dishes and imaged using DIC microscopy. Representative images are shown with insets from white boxes. Scale bar = 25 µm.

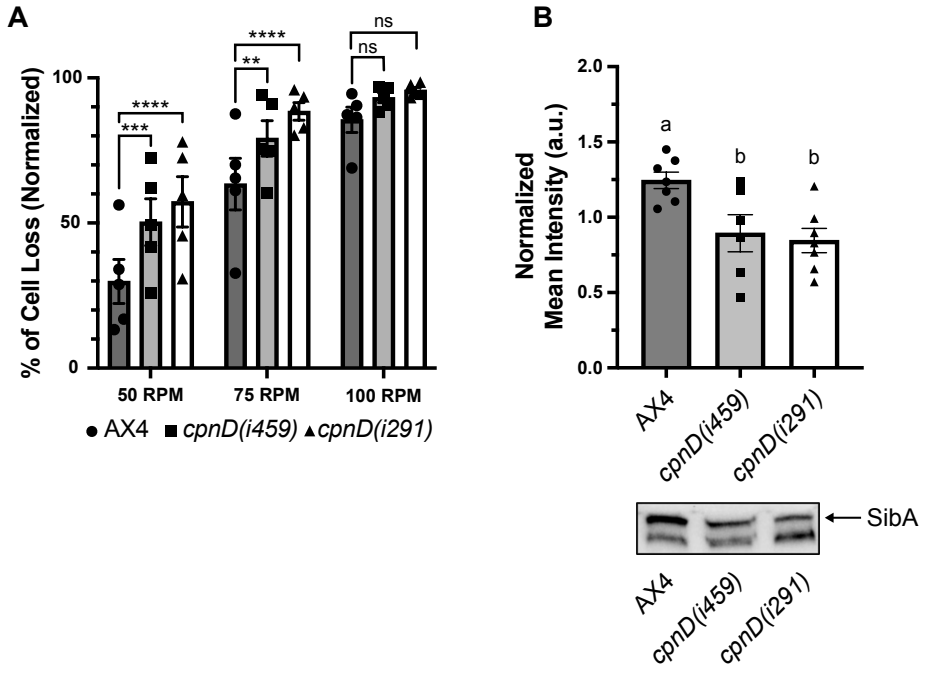

Figure 4. *cpnD* mutants have reduced cell-substrate adhesion and SibA expression. (A) AX4 and *cpnD* mutant cell lines were plated on 60 mm Petri dishes. Cells were imaged with phase-contrast microscopy at three marked spots before and after rotation at 50, 75, and 100 RPM. The number of cells in each image was counted and averaged. The percentage of detached cells after rotation was calculated by subtracting the average number of cells remaining after each rotation from the average number of cells present before rotation, divided by the number of cells present before rotation. Data from five trials were averaged and analyzed for significant differences between the AX4 and *cpnD* mutant cell lines using a repeated measures two-way ANOVA with uncorrected Fisher's LSD post hoc test. ** indicates $p < 0.01$, *** indicates $p < 0.001$, **** indicates $p < 0.0001$, ns indicates no significant difference. (B) Densitometry analysis of the SibA band on Western blots. The mean intensity of the SibA Western blot band from AX4 and *cpnD* mutants was normalized to their respective lanes on stain-free gel images. The bar graph represents the average normalized band densities from 6 trials, and these data were analyzed for significant differences using a one-way ANOVA with Tukey's post hoc multiple comparisons test. Different letters indicate a significant difference ($p < 0.05$) while the same letters indicate no significant difference. A representative Western blot analysis of SibA expression in AX4 and *cpnD* mutant cells is included below the bar graph.

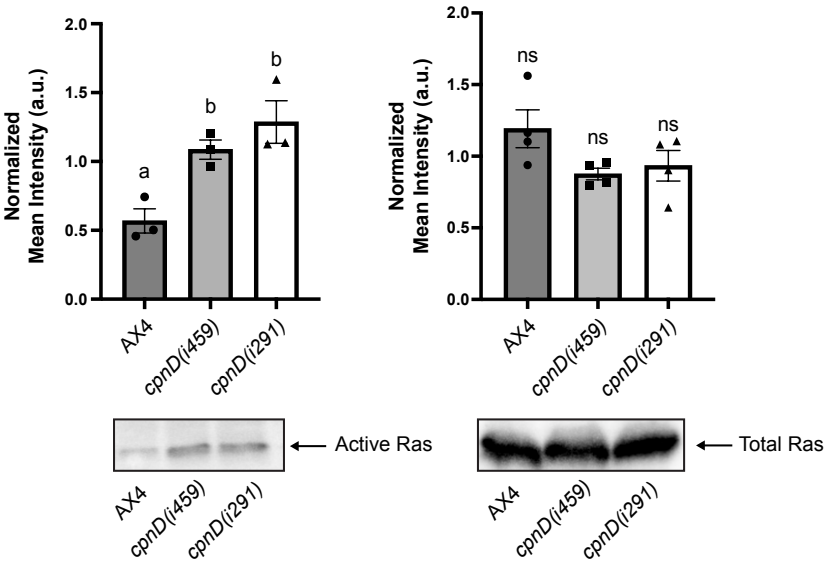

Figure 5. *cpnD* mutants have increased levels of activated Ras. Densitometry analysis of the activated and total Ras bands on Western blots. The mean intensity of total Ras alone was measured and normalized to the density of all proteins in the corresponding lane from the stain-free gel image. Normalized Western blot band densities were further normalized to the average adjusted total band volume intensities across all lanes. Data were analyzed across four trials, and significant differences were determined using a one-way ANOVA with Tukey's post hoc multiple comparisons test. ns indicates no significant difference. The adjusted total band volume densities of the activated Ras Western blot bands from AX4 and *cpnD* mutants were normalized to the average adjusted total band volume intensities across all active Ras lanes, as mentioned above. Normalized active Ras band densities were further normalized to the normalized adjusted total band volume intensities of their respective total Ras samples. Data were analyzed across three trials, and significant differences were determined using a one-way ANOVA with Tukey's post hoc multiple comparisons test. Different letters above the bars indicate significant differences ($p < 0.05$), while the same letter indicates no significant difference. Representative Western blot analyses of active Ras and total Ras are shown below their respective bar graphs.

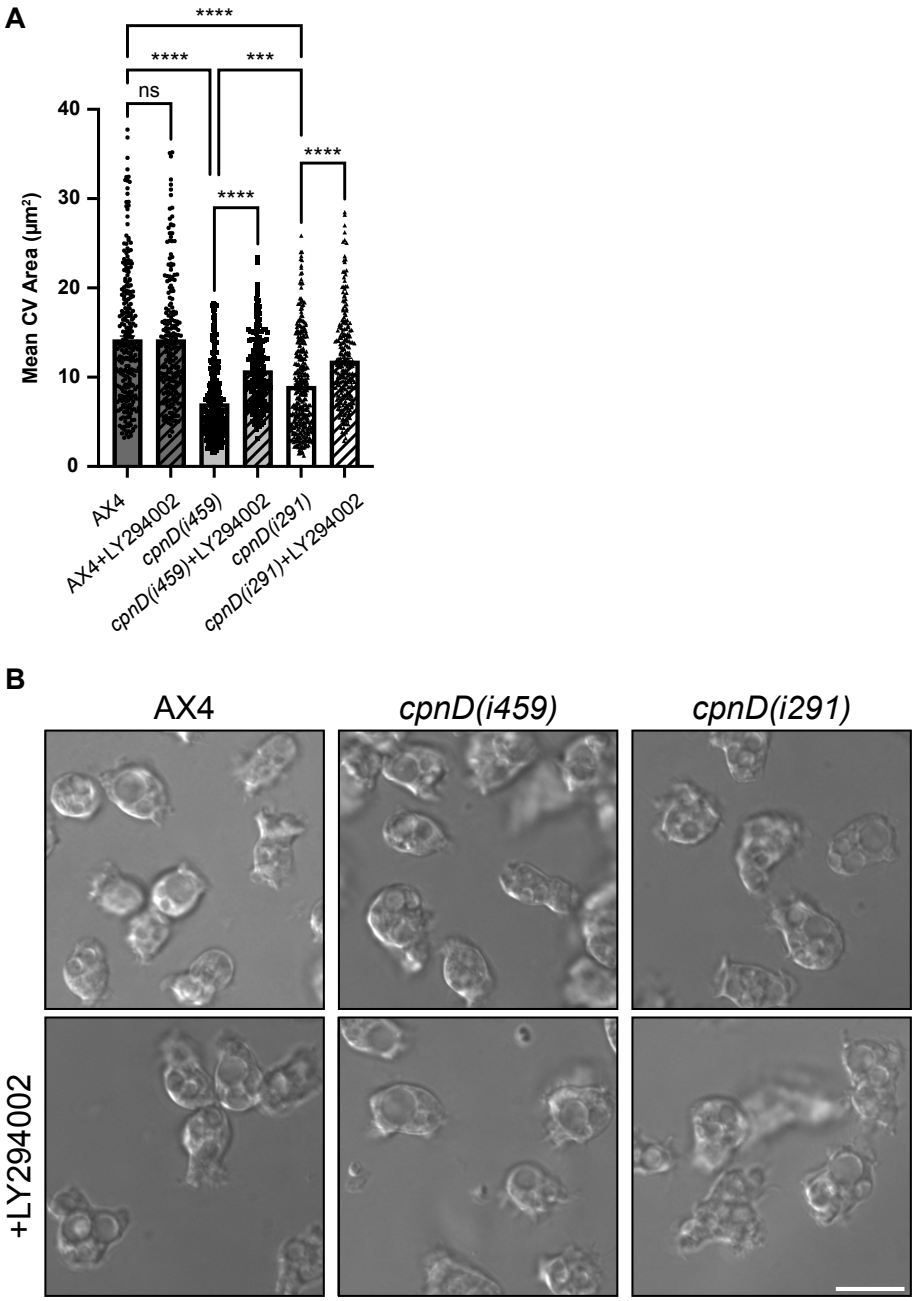

Figure 6. *cpnD* mutant cells have significantly smaller contractile vacuoles. (A) AX4 and *cpnD* mutant cells were plated on glass-bottom dishes and incubated in water in the absence or presence of 25 μM PI3K inhibitor (LY294002). The mean area of CVs (n > 209 CVs per cell line) was measured using ImageJ. After removing outliers, the data across two trials were analyzed for significant differences using a one-way ANOVA with Šídák's post hoc multiple comparisons test. *** indicates $p < 0.001$, **** indicates $p < 0.0001$. ns indicates no significant difference. (B) Representative images of CVs in the AX4 and *cpnD* mutant cell lines in the absence and presence of LY294002. Scale bar = 20 μm.

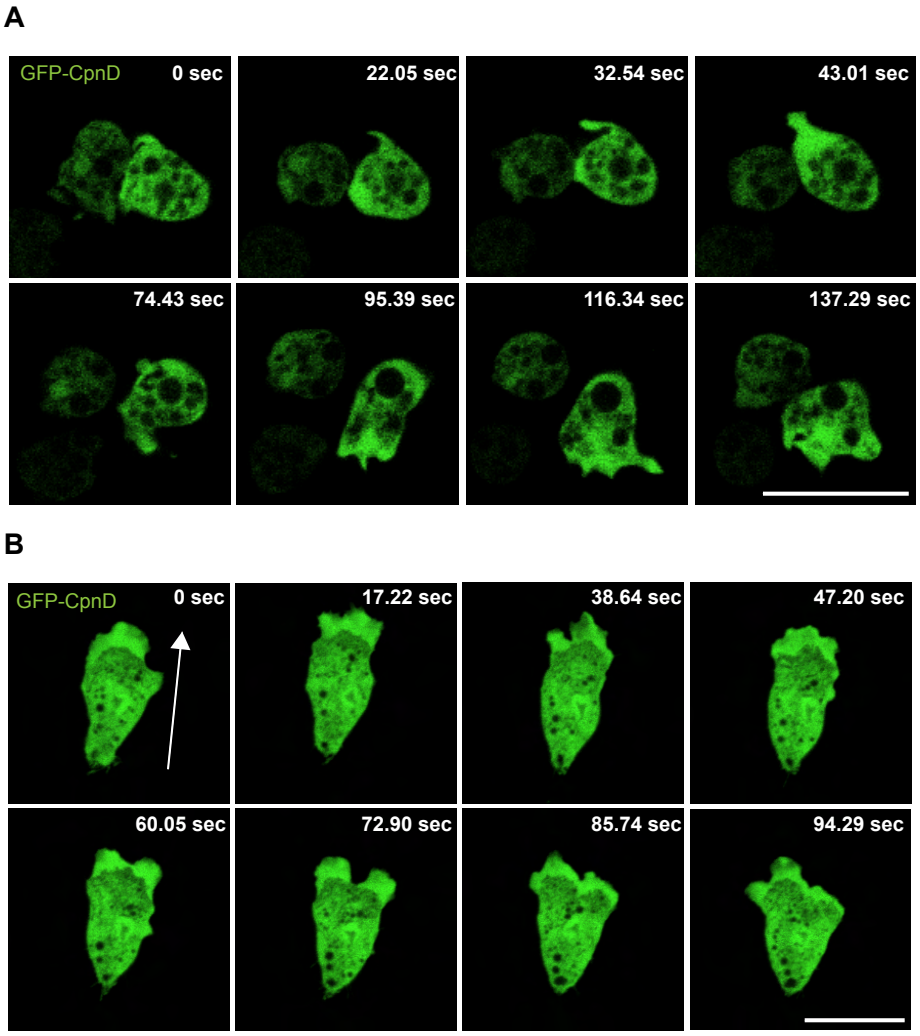

Figure 7. GFP-tagged CpnD localizes to the leading edge in both randomly migrating cells and in response to folate. (A) Cells expressing GFP-tagged CpnD were allowed to adhere to glass-bottom dishes before being imaged using time-lapse confocal microscopy. Scale bar = 20 μm. (B) Cells expressing GFP-tagged CpnD were allowed to crawl under agar towards folate before time-lapse confocal microscopy. Arrow points in the direction of folate. Scale bar = 20 μm.

References

1. Creutz CE, Tomsig JL, Snyder SL, Gautier MC, Skouri F, Beisson J, et al. The copines, a novel class of C2 domain-containing, calcium-dependent, phospholipid-binding proteins conserved from Paramecium to humans. J Biol Chem. 1998;273(3):1393–402. doi:10.1074/jbc.273.3.1393

2. Tomsig JL, Creutz CE. Copines: a ubiquitous family of Ca2+-dependent phospholipid-binding proteins. Cell Mol Life Sci. 2002;59(9):1467–77. doi:10.1007/s00018-002-8522-7

3. Tang H, Pang P, Qin Z, Zhao Z, Wu Q, Song S, et al. The CPNE Family and Their Role in Cancers. Front Genet [Internet]. 2021;12. Available from: https://www.frontiersin.org/articles/10.3389/fgene.2021.689097

4. Nagasawa S, Ikeda K, Horie-Inoue K, Sato S, Itakura A, Takeda S, et al. Systematic Identification of Characteristic Genes of Ovarian Clear Cell Carcinoma Compared with High-Grade Serous Carcinoma Based on RNA-Sequencing. Int J Mol Sci. 2019;20(18):4330. doi:10.3390/ijms20184330

5. Han Y xiu, Tao C, Gao X ran, Wang L le, Jiang F hao, Wang C, et al. BDNF-Related Imbalance of Copine 6 and Synaptic Plasticity Markers Couples With Depression-Like Behavior and Immune Activation in CUMS Rats. Front Neurosci. 2018;12:731. doi:10.3389/fnins.2018.00731

6. Zhu B, Zha J, Long Y, Hu X, Chen G, Wang X. Increased expression of copine VI in patients with refractory epilepsy and a rat model. J Neurol Sci. 2016;360:30–6. doi:10.1016/j.jns.2015.11.041

7. Sakthivel KM, Prabhu VV. Copine 3 as a Novel Potential Drug Target for Non-Small-Cell Lung Carcinoma. Journal of Environmental Pathology, Toxicology and Oncology. 2017;36(2). doi:10.1615/JEnvironPatholToxicolOncol.2017019540

8. Jiang Z, Jiang J, Zhao B, Yang H, Wang Y, Guo S, et al. CPNE1 silencing inhibits the proliferation, invasion and migration of human osteosarcoma cells. Oncol Rep. 2018;39(2):643–50. doi:10.3892/or.2017.6128

9. Ahmat Amin MKB, Shimizu A, Zankov DP, Sato A, Kurita S, Ito M, et al. Epithelial membrane protein 1 promotes tumor metastasis by enhancing cell migration via copine-III and Rac1. Oncogene. 2018;37(40):5416–34. doi:10.1038/s41388-018-0286-0

10. Chen Z, Jiang Z, Zhang W, He B. Silencing the expression of copine-III enhances the sensitivity of hepatocellular carcinoma cells to the molecular targeted agent sorafenib. Cancer Manag Res. 2018;10:3057–67. doi:10.2147/CMAR.S167781

11. Liu P, Khvotchev M, Li YC, Chanaday NL, Kavalali ET. Copine-6 Binds to SNAREs and Selectively Suppresses Spontaneous Neurotransmission. The Journal of Neuroscience. 2018;38(26):5888–99. doi:10.1523/JNEUROSCI.0461-18.2018

12. Damer CK, Bayeva M, Hahn ES, Rivera J, Socec CI. Copine A, a calcium-dependent membrane-binding protein, transiently localizes to the plasma membrane and intracellular vacuoles in Dictyostelium. BMC Cell Biol. 2005;6:46. doi:10.1186/1471-2121-6-46

13. Kessin RH. Dictyostelium: Evolution, Cell Biology, and the Development of Multicellularity. Developmental and Cell Biology Series [Internet]. Cambridge: Cambridge University Press; 2001. Available from: https://www.cambridge.org/core/books/dictyostelium/4516B23DDBF5620A3965A5E3B14E83DF

14. Kortholt A, Keizer-Gunnink I, Kataria R, Van Haastert PJM. Ras activation and symmetry breaking during Dictyostelium chemotaxis. J Cell Sci. 2013;126(19):4502–13. doi:10.1242/jcs.132340

15. Kae H, Lim CJ, Spiegelman GB, Weeks G. Chemoattractant-induced Ras activation during Dictyostelium aggregation. EMBO Rep. 2004;5(6):602–6. doi:10.1038/sj.embor.7400151

16. Bolourani P, Spiegelman GB, Weeks G. Delineation of the roles played by RasG and RasC in cAMP-dependent signal transduction during the early development of Dictyostelium discoideum. Mol Biol Cell. 2006 Oct;17(10):4543–50. doi:10.1091/MBC.E05-11-1019 PubMed PMID: 16885420.

17. Chattwood A, Bolourani P, Weeks G. RasG signaling is important for optimal folate chemotaxis in Dictyostelium. BMC Cell Biol. 2014 Apr 17;15(1). doi:10.1186/1471-2121-15-13 PubMed PMID: 24742374.

18. Seastone DJ, Zhang L, Buczynski G, Rebstein P, Weeks G, Spiegelman G, et al. The small Mr Ras-like GTPase Rap1 and the phospholipase C pathway act to regulate phagocytosis in Dictyostelium discoideum. Mol Biol Cell. 1999;10(2):393–406. doi:10.1091/MBC.10.2.393 PubMed PMID: 9950684.

19. Jaiswal P, Meena NP, Chang FS, Liao XH, Kim L, Kimmel AR. An integrated, cross-regulation pathway model involving activating/adaptive and feed-forward/feed-back loops for directed oscillatory cAMP signal-relay/response during the development of Dictyostelium. Front Cell Dev Biol. 2023;11:1263316. doi:10.3389/FCELL.2023.1263316/FULL

20. Cai H, Das S, Kamimura Y, Long Y, Parent CA, Devreotes PN. Ras-mediated activation of the TORC2-PKB pathway is critical for chemotaxis. J Cell Biol. 2010 Jul 26;190(2):233–45. doi:10.1083/JCB.201001129 PubMed PMID: 20660630.

21. Artemenko Y, Lampert TJ, Devreotes PN. Moving towards a paradigm: common mechanisms of chemotactic signaling in Dictyostelium and mammalian leukocytes. Cell Mol Life Sci. 2014;71(19):3711. doi:10.1007/S00018-014-1638-8 PubMed PMID: 24846395.

22. Zhang S, Charest PG, Firtel RA. Spatiotemporal Regulation of Ras Activity Provides Directional Sensing. Current Biology. 2008 Oct 28;18(20):1587–93. doi:10.1016/j.cub.2008.08.069 PubMed PMID: 18948008.

23. Edwards M, Cai H, Abubaker-Sharif B, Long Y, Lampert TJ, Devreotes PN. Insight from the maximal activation of the signal transduction excitable network in Dictyostelium discoideum. Proc Natl Acad Sci U S A. 2018 Apr 17;115(16):E3722–30. doi:10.1073/PNAS.1710480115/SUPPL_FILE/PNAS.1710480115.SM11.AVI PubMed PMID: 29602807.

24. Lin Y, Pal DS, Banerjee P, Banerjee T, Qin G, Deng Y, et al. Ras suppression potentiates rear actomyosin contractility-driven cell polarization and migration. Nat Cell Biol. 2024 Jul 1;26(7):1062–76. doi:10.1038/S41556-024-01453-4 PubMed PMID: 38951708.

25. Pylayeva-Gupta Y, Grabocka E, Bar-Sagi D. RAS oncogenes: weaving a tumorigenic web. Nat Rev Cancer. 2011 Nov;11(11):761–74. doi:10.1038/NRC3106 PubMed PMID: 21993244.

26. Cox AD, Fesik SW, Kimmelman AC, Luo J, Der CJ. Drugging the undruggable RAS: Mission Possible? Nature Reviews Drug Discovery 2014 13:11. 2014 Oct 17;13(11):828–51. doi:10.1038/nrd4389 PubMed PMID: 25323927.

27. Downward J. Targeting RAS signalling pathways in cancer therapy. Nat Rev Cancer. 2003 Jan;3(1):11–22. doi:10.1038/NRC969 PubMed PMID: 12509763.

28. Damer CK, Bayeva M, Kim PS, Ho LK, Eberhardt ES, Socec CI, et al. Copine A is required for cytokinesis, contractile vacuole function, and development in Dictyostelium. Eukaryot Cell. 2007 Mar;6(3):430–42. doi:10.1128/EC.00322-06/SUPPL_FILE/DAMERSMLEGENDS.DOC PubMed PMID: 17259548.

29. Ilacqua AN, Price JE, Graham BN, Buccilli MJ, McKellar DR, Damer CK. Cyclic AMP signaling in Dictyostelium promotes the translocation of the copine family of calcium-binding proteins to the plasma membrane. BMC Cell Biol. 2018;19(1):13. doi:10.1186/s12860-018-0160-5

30. Buccilli MJ, Ilacqua AN, Han M, Banas AA, Wight EM, Mao H, et al. Copine A Interacts with Actin Filaments and Plays a Role in Chemotaxis and Adhesion. Cells. 2019;8(7):758. doi:10.3390/cells8070758

31. Wight EM, Ide AD, Damer CK. Copine A regulates the size and exocytosis of contractile vacuoles and postlysosomes in Dictyostelium. FEBS Open Bio. 2020;10(6):979–94. doi:10.1002/2211-5463.12874

32. Ide AD, Wight EM, Damer CK. Phosphatidylserine exposure promotes increased adhesion in Dictyostelium Copine A mutants. PLoS One. 2021;16(5):e0250710. doi:10.1371/journal.pone.0250710

33. Ide AD, Morrison CT, Carne CA, Damer CK. Copine A is essential for calcium homeostasis in Dictyostelium. Cell Calcium. 2025 Sep 1;130:103055. doi:10.1016/J.CECA.2025.103055

34. Nichols RA, Ide AD, Morrison CT, Anger AL, Buccilli MJ, Damer CK. Copine C plays a role in adhesion and streaming in Dictyostelium. Cell Adh Migr. 2024 May 11;18(1):1–19. doi:10.1080/19336918.2024.2315629

35. Fey P, Dodson RJ, Basu S, Chisholm RL. One stop shop for everything Dictyostelium: dictyBase and the Dicty Stock Center in 2012. Methods Mol Biol. 2013;983:59–92. doi:10.1007/978-1-62703-302-2_4 PubMed PMID: 23494302.

36. Gruenheit N, Baldwin A, Stewart B, Jaques S, Keller T, Parkinson K, et al. Mutant resources for functional genomics in Dictyostelium discoideum using REMI-seq technology. BMC Biol. 2021;19(1):172. doi:10.1186/s12915-021-01108-y

37. Dias M, Brochetta C, Marchetti A, Bodinier R, Brückert F, Cosson P. Role of SpdA in Cell Spreading and Phagocytosis in Dictyostelium. PLoS One. 2016 Aug 1;11(8). doi:10.1371/JOURNAL.PONE.0160376 PubMed PMID: 27512991.

38. Mijanović L, Putar D, Mimica L, Klajn S, Filić V, Weber I. The IQGAP-related RasGAP IqgC regulates cell-substratum adhesion in Dictyostelium discoideum. Cell Mol Biol Lett. 2025 Dec 1;30(1). doi:10.1186/S11658-024-00678-3 PubMed PMID: 39789437.

39. Cornillon S, Froquet R, Cosson P. Involvement of Sib proteins in the regulation of cellular adhesion in Dictyostelium discoideum. Eukaryot Cell. 2008 Sep;7(9):1600–5. doi:10.1128/EC.00155-08 PubMed PMID: 18676957.

40. Kortholt A, Kataria R, Keizer-Gunnink I, Van Egmond WN, Khanna A, Van Haastert PJM. Dictyostelium chemotaxis: essential Ras activation and accessory signalling pathways for amplification. EMBO Rep. 2011 Dec;12(12):1273. doi:10.1038/EMBOR.2011.210 PubMed PMID: 22081140.

41. Lin Y, Parajón E, Yuan Q, Ye S, Qin G, Deng Y, et al. Ras-mediated dynamic and biphasic regulation of cell migration. Proc Natl Acad Sci U S A. 2025 Jul 29;122(30):e2503847122. doi:10.1073/PNAS.2503847122;SUBPAGE:STRING:FULL PubMed PMID: 40694332.

42. Gabriel D, Hacker U, Köhler J, Müller-Taubenberger A, Schwartz JM, Westphal M, et al. The contractile vacuole network of Dictyostelium as a distinct organelle: its dynamics visualized by a GFP marker protein. J Cell Sci. 1999;112 (Pt 22)(22):3995–4005. doi:10.1242/JCS.112.22.3995 PubMed PMID: 10547360.

43. Veeranki S, Kim B, Kim L. The GPI-anchored superoxide dismutase SodC is essential for regulating basal Ras activity and for chemotaxis of Dictyostelium discoideum. J Cell Sci. 2008 Sep 15;121(18):3099–108. doi:10.1242/JCS.030056 PubMed PMID: 18768936.

44. Castellano E, Downward J. Role of RAS in the Regulation of PI 3-Kinase [Internet]. 2010;143–69. doi:10.1007/82_2010_56

45. Bozzaro S, Eichinger L. The Professional Phagocyte Dictyostelium discoideum as a Model Host for Bacterial Pathogens. Curr Drug Targets. 2011 Nov 1;12(7):942. doi:10.2174/138945011795677782 PubMed PMID: 21366522.

46. Peracino B, Balest A, Bozzaro S. Phosphoinositides differentially regulate bacterial uptake and Nramp1-induced resistance to Legionella infection in Dictyostelium. J Cell Sci. 2010 Dec 1;123(23):4039–51. doi:10.1242/JCS.072124 PubMed PMID: 21045112.

47. Stephens L, Ellson C, Hawkins P. Roles of PI3Ks in leukocyte chemotaxis and phagocytosis. Curr Opin Cell Biol. 2002 Apr 1;14(2):203–13. doi:10.1016/S0955-0674(02)00311-3 PubMed PMID: 11891120.

48. Xu X, Pots H, Gilsbach BK, Parsons D, Veltman DM, Ramachandra SG, et al. C2GAP2 is a common regulator of Ras signaling for chemotaxis, phagocytosis, and macropinocytosis. Front Immunol. 2022 Nov 29;13:1075386. doi:10.3389/FIMMU.2022.1075386/TEXT PubMed PMID: 36524124.

49. Bolourani P, Spiegelman G, Weeks G. Ras Proteins Have Multiple Functions in Vegetative Cells of Dictyostelium. Eukaryot Cell. 2010 Nov;9(11):1728. doi:10.1128/EC.00141-10 PubMed PMID: 20833893.

50. Sasaki AT, Chun C, Takeda K, Firtel RA. Localized Ras signaling at the leading edge regulates PI3K, cell polarity, and directional cell movement. J Cell Biol. 2004 Nov 8;167(3):505. doi:10.1083/JCB.200406177 PubMed PMID: 15534002.

51. Plak K, Keizer-Gunnink I, J M Van Haastert P, Kortholt A. Rap1-dependent pathways coordinate cytokinesis in Dictyostelium. Mol Biol Cell. 2014 Dec 15;25(25):4195. doi:10.1091/MBC.E14-08-1285 PubMed PMID: 25298405.

52. Jeon TJ, Lee DJ, Merlot S, Weeks G, Firtel RA. Rap1 controls cell adhesion and cell motility through the regulation of myosin II. J Cell Biol. 2007 Mar 26;176(7):1021. doi:10.1083/JCB.200607072 PubMed PMID: 17371831.

53. Kortholt A, van Haastert PJM. Highlighting the role of Ras and Rap during Dictyostelium chemotaxis. Cell Signal. 2008 Aug 1;20(8):1415–22. doi:10.1016/J.CELLSIG.2008.02.006 PubMed PMID: 18385017.

54. Sasaki AT, Firtel RA. Regulation of chemotaxis by the orchestrated activation of Ras, PI3K, and TOR. Eur J Cell Biol. 2006 Sep 27;85(9–10):873–95. doi:10.1016/j.ejcb.2006.04.007 PubMed PMID: 16740339.

55. Reinhard JR, Kriz A, Galic M, Angliker N, Rajalu M, Vogt KE, et al. The calcium sensor Copine-6 regulates spine structural plasticity and learning and memory. Nat Commun. 2016 May 19;7:11613. doi:10.1038/NCOMMS11613 PubMed PMID: 27194588.

56. Levi S, Polyakov M, Egelhoff TT. Green Fluorescent Protein and Epitope Tag Fusion Vectors for Dictyostelium discoideum. Plasmid. 2000 Nov 1;44(3):231–8. doi:10.1006/PLAS.2000.1487 PubMed PMID: 11078649.

57. Thomason PA, Traynor D, Cavet G, Chang WT, Harwood AJ, Kay RR. An intersection of the cAMP/PKA and two-component signal transduction systems in Dictyostelium. EMBO J. 1998 May 15;17(10):2838–45. doi:10.1093/EMBOJ/17.10.2838 PubMed PMID: 9582277.